Nonequilibrium radiation and dissociation of CO molecules in shock-heated flows

R. L. Macdonald,[1] A. Munafò,[1] C. O. Johnston,[2] and M. Panesi[1,*]
[1]*University of Illinois at Urbana-Champaign, Urbana, Illinois, USA*
[2]*NASA Langley Research Center, Hampton, Virginia, USA*
(Received 19 January 2016; published 1 August 2016)

This work addresses the study of the behavior of the excited electronic states of CO molecules in the nonequilibrium relaxation zone behind a normal shock for a CO_2-N_2 mixture representative of the Mars atmosphere. The hybrid state-to-state (StS) model developed accounts for thermal nonequilibrium between the translational energy mode of the gas and the vibrational energy mode of individual molecules. The electronic states of CO molecules are treated as separate species, allowing for non-Boltzmann distributions of their populations. The StS model is coupled with a nonequilibrium radiation solver, HPC-RAD, allowing for the calculation of the radiation signature from the molecular and atomic species in the gas. This study focuses on the radiation from the fourth positive system of CO, which dominates the radiation heating on the forebody for higher speed Mars entry applications. In the rapidly dissociating regime behind strong shock waves, the population of the ground electronic state of CO [$CO(X^1\Sigma)$], departs from Maxwell-Boltzmann distributions, owing to the efficient collisional excitation to the electronically excited $CO(A^1\Pi)$ state. In general the assumption of the equilibrium between electronic and vibration fails when the excitation of electronic states is driven by heavy particles. The comparison of the radiation heating predictions obtained using the conventional quasi-steady-state (QSS) approach and the physics-based StS approach revealed differences in radiative heating predictions of up to 50%. These results demonstrate that the choice of nonequilibrium model can have a significant impact on radiative heating simulations, and more importantly, they cast serious doubts on the validity of the QSS assumption for the condition of interest to this work.

DOI: 10.1103/PhysRevFluids.1.043401

I. INTRODUCTION

Modeling of the aero-thermal environment surrounding an entry vehicle, during its descent into a planetary atmosphere, is a very challenging task, due to the complex interaction of fluid dynamics, chemical kinetics, and radiation [1–3]. Mars entry is characterized by speeds between 6 and 8 km/s. At these entry velocities, the degree of ionization of the gas in the shock layer is negligibly small, and the nonequilibrium collisional kinetics is dominated by heavy-particle-driven processes (e.g., collisional excitation and dissociation). This constitutes an additional complication due to the inherent difficulty in computing or measuring transition probabilities for these processes.

Mars's atmosphere is composed in large part by CO_2 (96% X_{CO_2}), with a modest concentration of N_2 molecules (4% X_{N2}). The dissociation of CO_2 and N_2 molecules behind the bow shock leads to the formation of strong radiators such as CO and CN. By hindering the dissociation of these molecules nonequilibrium phenomena provoke an excess of radiators in the gas, thus enhancing the radiation field [4,5]. This fact has been known since the early experiments by Arnold *et al.* [6] and Nealy [7] and has been further confirmed by the recent calculations of Park *et al.* [4] and Johnston *et al.* [8]. The main contribution to the radiative heating is due to the CO fourth positive system (i.e., $A^1\Pi - X^1\Sigma^+$) [9]. Thus, the accurate determination of the concentration of the excited states of CO is crucial to the determination of the radiative heat loads during Mars entry.

*mpanesi@illinois.edu

Early attempts to model the aero-thermal environment in a shock-heated Martian atmosphere assumed an equilibrium Maxwell-Boltzmann distribution for the internal states of gas particles [4,10,11]. Park presented the first analysis of the nonequilibrium characteristics behind a shock wave relevant to Mars atmospheric entry. The analysis was based on the two-temperature model developed earlier by the same author [12,13] and used the most accurate kinetic data available at the time. Recently more sophisticated models have been developed to address some of the shortcomings of the Park model. For instance, Refs. [3,14–23] investigate the coupling between chemistry and internal energy relaxation (e.g., vibrational energy) in zero, one, and multidimensional flow configurations; Ref. [24] focused on the correct modeling of electronic excitation by using finite rate chemistry for the excited states of strong radiators (i.e., collisional-radiative models).

The experimental investigations of Rond, Lee, and Gorelov [16,25,26] have demonstrated the inadequacies of current models showing how kinetic data as well as nonequilibrium models are not accurate when used in the high temperature, nonequilibrium regimes.

More recently, Johnston *et al.* [27] proposed a new kinetic model for CO_2-N_2 mixture, which was calibrated and validated using the data acquired at the Electric Arc Shock Tube (EAST) facility at NASA Ames Research Center. The kinetic mechanism included processes for ground as well as electronically excited species, with the exception of dissociation from the excited states of CO molecules, which were purposefully left out. The analysis of the electronic nonequilibrium carried out in Johnston's work relies on the quasi-steady-state (QSS) assumption [12,28], which may not hold true in the Mars entry conditions.

The purpose of this paper is twofold: (1) improve the modeling of nonequilibrium dissociation of CO in order to account for the electronic excitation and (2) assess the validity of the QSS assumption.

Dissociation from electronically excited states: CO has a large number of electronic states below its dissociation limit. These electronic states constitute one of the most complex kinetic problems to study, owing to the large number of relaxation channels that become available in such a dense manifold of energy states [29]. A limited amount of data are available for the dissociation from the electronically excited states. Park [30] provides state-specific dissociation rates for electronic states, by scaling the ground states based on the well depth of each potential energy curve. It was found that the resulting global rate coefficient is overestimated by one order of magnitude with respect to the available experimental data. In this work, the method discussed by Aliat *et al.* in Ref. [31] is used to scale the global dissociation rate coefficient extracted by Johnston using EAST data.

QSS assumption: The QSS approach assumes that the magnitudes of the replenishing and depleting rates for a generic internal state (e.g., electronic, vibronic) are much larger than their difference. This allows us to set the net production rate to zero and, thus, to compute the population of excited states by simply postprocessing the flow field. The use of the QSS assumption is, on the one hand, computationally attractive, as it avoids for tracking the evolution of the population of excited states while computing the flow field. On the other hand, it is known that the QSS assumption does not hold true in general. The inaccuracies of QSS-based models led to the development of state-to-state (StS) or collisional-radiative (CR) models [32–34]. StS models couple the excited state kinetics with the flow field by considering the excited states as separate *pseudospecies* governed by their own kinetics. The StS approach can be applied to model the evolution of electronic [21,32,35–40], vibrational [18,41–45], or rovibrational states [46–49], with increasing complexity, and requirements in terms of computational cost.

The paper is organized as follows. Section II describes the physical model and the numerical method. The details of the kinetics, thermodynamics, and radiation are given in the Supplemental Material [50]. Results are discussed and analyzed in Sec. III. Additional test cases can be found in the Supplemental Material [50]. Conclusions are given in Sec. IV.

II. PHYSICAL MODELING

The present section describes in detail the physical model. The thermodynamic properties of the model Martian atmosphere considered in this work are treated in Sec. II A. Section II B deals

TABLE I. Electronic states of CO.

State	Term	g	E [cm^{-1}]
1	$X\,^1\Sigma^+$	1	0
2	$a\,^3\Pi$	6	48687
3	$a'\,^3\Sigma^+$	3	55836
4	$d\,^3\Delta$	6	61120
5	$e\,^3\Sigma^-$	6	64230
6	$A\,^1\Pi$	2	65076

with the collisional kinetic processes and the calculation of the related rate coefficients and energy transfer terms. The modeling of CO radiation is described in Sec. II C. The governing equations for the flow and radiation transport are given in Sec. II D.

A. Thermodynamics

Gas mixture. The Martian mixture considered in the present study consists of carbon dioxide, molecular nitrogen, and the products of their reactions. The chemical components are N, O, C, CO, CO_2, O_2, CN, N_2, NO, and O_2 as well as electrons, e^-, and singly charged positive ions, C^+, O^+, NO^+, O_2^+, and CO^+. Following the StS approach, six electronic levels of CO are explicitly introduced as separate *pseudospecies* in the mixture (see Table I). Coupling of the CO electronic energy levels through the different elementary processes considered in the following section allows for explicit determination of their excitation and the radiative signature of the plasma without using any *a priori* assumption on their populations. The vibrational and electronic energies of the other chemical components (e.g., C, CN, O_2, N_2, ...) are described by a Maxwell-Boltzmann distribution by using a common *vibronic* temperature T_{ve} [12]. The same temperature is used to account for thermal nonequilibrium between heavy particles and free electrons [12,38,51]. Rotational nonequilibrium effects are neglected.

For the sake of later convenience, we define the following sets, $\mathcal{S}_a$ and $\mathcal{S}_m$, which include, respectively, the atomic and molecular species and read $\mathcal{S}_a = \{C,O,N,C^+,O^+\}$ and $\mathcal{S}_m = \{CO(1-6),CO_2,O_2,CN,N_2,NO,O_2,NO^+,O_2^+,CO^+\}$, where the notation $CO(i)$ is introduced to denote the individual electronic levels of CO (stored in set $\mathcal{E}$). The heavy-particle and total species sets are $\mathcal{S}_h = \mathcal{S}_a \cup \mathcal{S}_m$ and $\mathcal{S} = \mathcal{S}_h \cup \{e^-\}$, respectively. The heavy particles not treated in StS are stored in set $\mathcal{S}_h^* = \mathcal{S}_h \setminus \mathcal{E}$.

Thermodynamic properties. The gas pressure is computed based on Dalton's law as $p = p_e + p_h$, where the free-electron and heavy-particle partial pressures are $p_e = n_e k_B T_{ve}$ and $p_h = n_h k_B T$, respectively, with the symbol k_B denoting the Boltzmann constant. Quantities n_e and n_h represent the number densities of free electrons and heavy particles, with the latter being defined as $n_h = \sum_{s\in\mathcal{S}_h} n_s$.

The gas thermal, rotational, vibronic, and free-electron energy densities are

$$\rho e = \frac{3}{2}p + \rho e_r + \rho e_{ev} + \sum_{s\in\mathcal{S}_h} n_s E_s^f, \tag{1}$$

$$\rho e_r = \sum_{m\in\mathcal{S}_m} n_m \tilde{E}_m^r(T), \tag{2}$$

$$\rho e_{elv} = \sum_{m\in\mathcal{S}_m} n_m \tilde{E}_m^v(T_{ve}) + \sum_{s\in\mathcal{S}_h^*} n_s \tilde{E}_s^{el}(T_{ve}) + \sum_{i\in\mathcal{E}} n_i E_i, \tag{3}$$

$$\rho e_e = \frac{3}{2}p_e. \tag{4}$$

The last sum in Eq. (3) represents the contribution of the electronic levels of CO. The former is kept separate from the electronic energy of the non-StS species [i.e., the second sum in Eq. (3)] for the sake of convenience (see Sec. II D). The particle rotational and vibrational energies ($\tilde{E}^{\mathrm{r}}_m$ and $\tilde{E}^{\mathrm{v}}_m$, $m \in \mathcal{S}_{\mathrm{m}}$, respectively) are computed, respectively, based on the rigid-rotor and harmonic-oscillator models. The particle electronic energies of the non-StS species [$\tilde{E}^{\mathrm{el}}_s(T_{\mathrm{ve}})$, $s \in \mathcal{S}^*_{\mathrm{h}}$] are computed under the assumption of a Boltzmann distribution at T_{ve} for the electronic levels. Spectroscopic data and formation energies (E^{f}_s, $s \in \mathcal{S}_{\mathrm{h}}$) needed to evaluate expressions (1)–(3) are taken from Gurvich tables [52].

B. Collisional processes

The kinetic model used in this paper is based on the work of Johnston *et al.* [27]. The processes considered were compiled from the best available sources [4,8,12,13,53–59] and account for heavy-particle impact reactions (e.g., dissociation, excitation, exchange, charge exchange, and associative ionization), and excitation and ionization by electron impact reactions. The kinetics of the electronic states of CO is modeled based on a StS approach and comprises the following:

(1) Excitation by electron and heavy-particle impact:

$$\mathrm{CO}(i) + \mathrm{M} \underset{k^{\mathrm{Exh}}_{ji(m)}}{\overset{k^{\mathrm{Exh}}_{ij(m)}}{\rightleftharpoons}} \mathrm{CO}(j) + \mathrm{M}, \quad \mathrm{CO}(i) + \mathrm{e}^- \underset{k^{\mathrm{Exe}}_{ji}}{\overset{k^{\mathrm{Exe}}_{ij}}{\rightleftharpoons}} \mathrm{CO}(j) + \mathrm{e}^-, \quad j > i; \tag{5}$$

(2) Dissociation by heavy-particle impact:

$$\mathrm{CO}(i) + \mathrm{M} \underset{k^{\mathrm{R}}_{i(m)}}{\overset{k^{\mathrm{D}}_{i(m)}}{\rightleftharpoons}} \mathrm{C} + \mathrm{O} + \mathrm{M}, \tag{6}$$

$i, j \in \mathcal{E}$, where the symbol M stands for a generic heavy collision partner. The acronyms Ex, D, and R have been introduced to denote, respectively, excitation, dissociation, and recombination (with the letters e and h used to distinguish between heavy-particle and electron-impact excitation). With the exception for the CO electronic excitation and dissociation reactions (5) and (6), the kinetic processes taken into account in this work have been modeled based on a multitemperature (MT) approach.

The calculations of the StS CO rate coefficients for excitation (5) and dissociation (6) (and the related master equation and QSS modeling) is detailed in Sec. II B 1. The calculation of the MT rate coefficients and energy transfer terms is outlined in Sec. II B 2.

1. CO electronic StS kinetic model

Master equation. The starting point of any StS model is represented by the master equation. This equation describes the time rate of change of the number of particles occupying a given energy state due to collisional-radiative transitions. In the case of the CO electronic excitation and dissociation processes (5) and (6) considered in this work, one has

$$\begin{aligned}\frac{\partial n_i}{\partial t} = &- \sum_{m\in\mathcal{S}_{\mathrm{h}}} \sum_{\substack{j\neq i \\ j\in\mathcal{E}}} n_m \left[n_i\, k^{\mathrm{Exh}}_{ij(m)}(T) - n_j\, k^{\mathrm{Exh}}_{ji(m)}(T) \right] - \sum_{\substack{j\neq i \\ j\in\mathcal{E}}} n_{\mathrm{e}} \left[n_i\, k^{\mathrm{Exe}}_{ij}(T_{\mathrm{ve}}) - n_j\, k^{\mathrm{Exe}}_{ji}(T_{\mathrm{ve}}) \right] \\ &- \sum_{m\in\mathcal{S}_{\mathrm{h}}} n_m \left[n_i\, k^{\mathrm{D}}_{i(m)}(T_{\mathrm{a}}) - n_{\mathrm{C}}\, n_{\mathrm{O}}\, k^{\mathrm{R}}_{i(m)}(T) \right], \quad i \in \mathcal{E},\end{aligned} \tag{7}$$

where T_{a} stands for the activation temperature for heavy-particle impact processes. The endothermic rate coefficients for de-excitation and recombination are obtained based on those for excitation and

dissociation, respectively, by means of detailed balance:

$$\frac{k^{\mathrm{Exh}}_{ji(m)}(T)}{k^{\mathrm{Exh}}_{ij(m)}(T)} = \frac{g_i}{g_j}\exp\left(\frac{E_j - E_i}{\mathrm{k_B}T}\right), \quad j > i, \tag{8}$$

$$\frac{k^{\mathrm{Exe}}_{ji}(T_{\mathrm{ve}})}{k^{\mathrm{Exe}}_{ij}(T_{\mathrm{ve}})} = \frac{g_i}{g_j}\exp\left(\frac{E_j - E_i}{\mathrm{k_B}T_{\mathrm{ve}}}\right), \quad j > i, \tag{9}$$

$$\frac{k^{\mathrm{R}}_{i(m)}(T)}{k^{\mathrm{D}}_{i(m)}(T)} = \left(\frac{\mathrm{h_P^2}}{2\pi\,\mathrm{k_B}T}\frac{m_{\mathrm{CO}}}{m_{\mathrm{C}}m_{\mathrm{O}}}\right)^{3/2}\frac{g_i\,\tilde{Q}^{\mathrm{r}}_{\mathrm{CO}}(T)\,\tilde{Q}^{\mathrm{v}}_{\mathrm{CO}}(T)}{\tilde{Q}^{\mathrm{el}}_{\mathrm{C}}(T)\,\tilde{Q}^{\mathrm{el}}_{\mathrm{O}}(T)}\exp\left(\frac{E^{\mathrm{f}}_{\mathrm{C}} + E^{\mathrm{f}}_{\mathrm{O}} - E^{\mathrm{f}}_{\mathrm{CO}} - E_i}{\mathrm{k_B}T}\right), \tag{10}$$

$i, j \in \mathcal{E}, m \in \mathcal{S}_{\mathrm{h}}$, where $\mathrm{h_P}$ stands for Planck's constant. The symbol m_s denotes the mass of species s. Quantities $\tilde{Q}^{\mathrm{r}}_s$, $\tilde{Q}^{\mathrm{v}}_s$, and $\tilde{Q}^{\mathrm{el}}_s$ represent, respectively, the rotational, vibrational, and electronic partition function of species s. The rate coefficients for excitation and dissociation have been evaluated as explained in the next two paragraphs.

Excitation rate coefficients. During Mars atmospheric entry (usually occurring between 6 and 8 km/s), the reactions with heavy particles dominate the kinetics because electrons are cold and their concentration is small. Nonetheless, determining rate coefficients for excited states in heavy-particle collisions constitutes a challenge both computationally and experimentally. Experimentally determining the rate coefficients requires knowledge about the full kinetic mechanism in the experimental setup. Furthermore, experiments are rarely done at high temperature and must be extrapolated to the temperatures of interest. Computationally, determining rate coefficients requires expensive quantum mechanical chemistry calculations, which are becoming more and more realistic, but still rely on several underlying assumptions about the collisions. In Refs. [30,60], Park has presented an overview of the electron and heavy-particle impact processes for electronic excited states of several molecules, including excitation and dissociation for CO. Unfortunately, most of the data is extrapolated from room temperature and has not been yet validated at high temperatures. Due to the lack of more reliable data, in the present work, Park's rates have been used to model electron and heavy-particle impact excitation of CO. For heavy-particle excitation, the activation temperature is taken at the geometric average between the heavy-particle translational temperature and the free-electron-vibrational temperature, $T_{\mathrm{a}} = \sqrt{T\,T_{\mathrm{ve}}}$.

Dissociation rate coefficients. The electronic state-specific dissociation rate coefficients of CO molecules have been computed using the approach proposed by Treanor *et al.* [61]. The Treanor-Marrone method allows for the estimation of the dissociation reaction coefficients based upon simple consideration of the kinematics of the collision. This method, originally developed for ground-state dissociation, has been extended by Aliat *et al.* [31] to account for dissociation from vibronic (v,i) states:

$$\mathrm{CO}(v,i) + \mathrm{M} \rightleftarrows \mathrm{C} + \mathrm{O} + \mathrm{M}. \tag{11}$$

The vibronic dissociation rate coefficients are obtained by multiplying the global dissociation rate coefficient ($k^{\mathrm{D}}_{(m)}$, $m \in \mathcal{S}_{\mathrm{h}}$) by the scaling factor V_{vi}:

$$V_{vi}(T,U) = \tilde{Q}^{\mathrm{el}}(T)\exp\left[\frac{E_{(v,i)}}{\mathrm{k_B}}\left(\frac{1}{T} + \frac{1}{U}\right)\right] \times \left[\sum_{i\in\mathcal{E}} g_i \exp\left(\frac{E_i}{\mathrm{k_B}U}\right)\frac{\tilde{Q}^{\mathrm{v}}_i(-U)}{\tilde{Q}^{\mathrm{v}}_i(T)}\right]^{-1}, \tag{12}$$

where $E_{(v,i)}$ stands for the energy of the vibronic state (v,i), and quantity $\tilde{Q}^{\mathrm{v}}_i$ denotes the vibrational partition function of the electronic state i. The parameter U (which has the dimension of a temperature) allows one to bias the dissociation to the high-lying vibrational states (e.g., the limiting case $U \to +\infty$ corresponds to the unbiased or equally probable dissociation from all vibrational states).

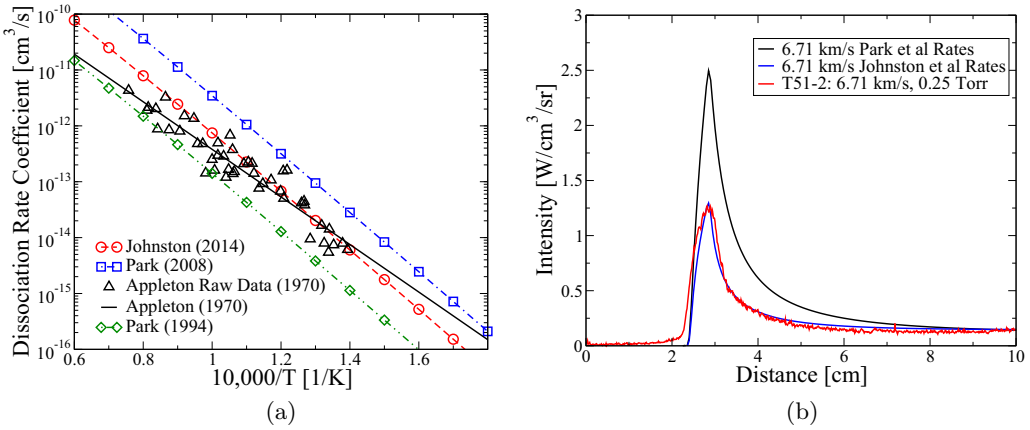

FIG. 1. Current dissociation models. (a) Global dissociation rates from Appleton [62], Johnston [27], and Park [30]. (b) Comparison of Park and Johnston models with EAST integrated intensity data [63].

To obtain the CO electronic dissociation rate coefficients, the vibronic rate coefficients, $k^{\mathrm{D}}_{(m)}(T)V_{vi}(T,U)$, are averaged over a Maxwell-Boltzmann distribution for the vibrational states:

$$k^{\mathrm{D}}_{i(m)}(T) = \frac{1}{\tilde{Q}^{\mathrm{v}}_i(T)} \sum_{v\in\mathcal{V}_i} k^{\mathrm{D}}_{(m)}(T)V_{vi}(T,U) \exp\left(-\frac{E^{\mathrm{v}}_{(v,i)}}{\mathrm{k_B}T}\right), \tag{13}$$

$i \in \mathcal{E}$, $m \in \mathcal{S}_{\mathrm{h}}$, where the vibrational energy of vibronic state (v,i) is $E^{\mathrm{v}}_{(v,i)} = E_{(v,i)} - E_i$. The set $\mathcal{V}_i$ stores the vibrational states of the electronic level i.

The vibronic dissociation rate coefficients, given in Eq. (13), depend on the choice of the global dissociation rate, $k^{\mathrm{D}}_{(m)}(T)$. Figure 1(a) compares the value of $k^{\mathrm{D}}_{(m)}(T)$ given by Appleton [62], Park [4,30], and Johnston [27] for a wide range of temperatures. Park's rates, indicated by the green and the blue curves, differ by more than one order of magnitude. The green results were estimated using Park's two-temperature model, as discussed in Ref. [4], while the blue curve was obtained by averaging Park's state-specific rates coefficient [30] over a Maxwell-Boltzmann distribution. This assumption results in an overestimation of the dissociation rate, since nonequilibrium effects tend to deplete the population of the high-lying electronic states. In this sense the blue curve can be considered the upper limit for the global dissociation rate.

More recently, Johnston derived a global dissociation rate by calibrating the Arrhenius parameters to reproduce radiation measurements collected on the EAST facility [27]. Figure 1(b) compares the radiation profiles obtained using Park and Johnston models against the experimental data collected on EAST shock tube [63]. The use of Park model leads to a large overestimation of the radiation intensity in the overshoot region located right behind the shock. The Johnston model yields a better prediction of the nonequilibrium overshoot region and appears to be in better agreement with Appleton data shown in Fig. 1(a). For these reasons Johnston's model was adopted in this work.

The StS CO rate coefficients obtained based on Eq. (13) have been fitted to a modified Arrhenius law:

$$k(T) = A\,T^{\eta}\exp(-\theta/T). \tag{14}$$

The fitting parameters A, η, and θ for the various electronic states and collision partners are provided in Table II.

Figure 2 shows the dissociation rate coefficients for different electronic states of CO. The rate coefficients strongly depend on the electronic level and appear to increase considerably for high-lying states. The rate coefficients used in the final model correspond to the $U = 3T$ case.

TABLE II. Fit coefficients for CO electronic state-specific dissociation rate coefficients.

	M = N, C, O			M = All Others		
Electronic State	A [cm^3 s^{-1}]	η	θ [K]	A [cm^3 s^{-1}]	η	θ [K]
$X\,^1\Sigma^+$	2.61×10^{-9}	0.19	123 661	1.74×10^{-9}	0.19	123 661
$a\,^3\Pi$	6.68×10^{-10}	0.26	52 873	4.45×10^{-9}	0.26	52 873
$a'\,^3\Sigma^+$	2.94×10^{-10}	0.33	42 633	1.96×10^{-10}	0.33	42 633
$d\,^3\Delta$	3.80×10^{-10}	0.30	34 217	2.54×10^{-10}	0.30	34 217
$e\,^3\Sigma^-$	1.31×10^{-10}	0.39	29 646	8.75×10^{-11}	0.39	29 646
$A\,^1\Pi$	6.04×10^{-11}	0.46	28 750	4.04×10^{-11}	0.46	28 750

QSS approach. The QSS approach is a complexity reduction technique developed to alleviate the computational cost associated with the solution of the set of master equations in the StS approach. In its conventional form it is composed of the following two steps:

(1) *Approximation of the master equation*. In this step, one postulates that the net mass production rate in Eq. (7) is negligibly small for a subset of equations (i.e., $\partial n_i/\partial t \simeq 0$) [12]. As a consequence, the (differential) set of master equations is reduced to a system of algebraic equations (see below).

(2) *Decoupling the excited state kinetics from the flow-field calculation*. The flow-field quantities, including the densities of the chemical components, are computed using a conventional MT model, and the populations of the excited states are solved for as a postprocessing step. The *corrected* population distributions can now be used in a radiation code for the evaluation of the optical properties of the plasma and the computation of radiative quantities of interest (e.g., average intensity, heat-flux).

In the case under consideration, the QSS assumption is adopted for all the excited states of CO(2–6). The final equation required to close the system is obtained by imposing the constraint of conservation of the total number of particles, $n_{\mathrm{CO}} = \sum_{i\in\mathcal{E}} n_i$, where the global CO number density, n_{CO}, is obtained from a MT solution. To avoid poor numerical conditioning in the obtained set of algebraic equations (which is linear in the present case), Park [12] suggests introducing the partial equilibrium dissociation and (Saha) ionization number densities (n_i^{D} and n_i^{I}, respectively) and to solve for the scaled unknowns $x_i = n_i/n_i^{\mathrm{I}}$. Once this transformation is performed, the QSS linear algebraic system can be written as, $\mathbf{Ax} = \mathbf{b}$, where the entries of left-hand-side matrix $\mathbf{A}$ and the

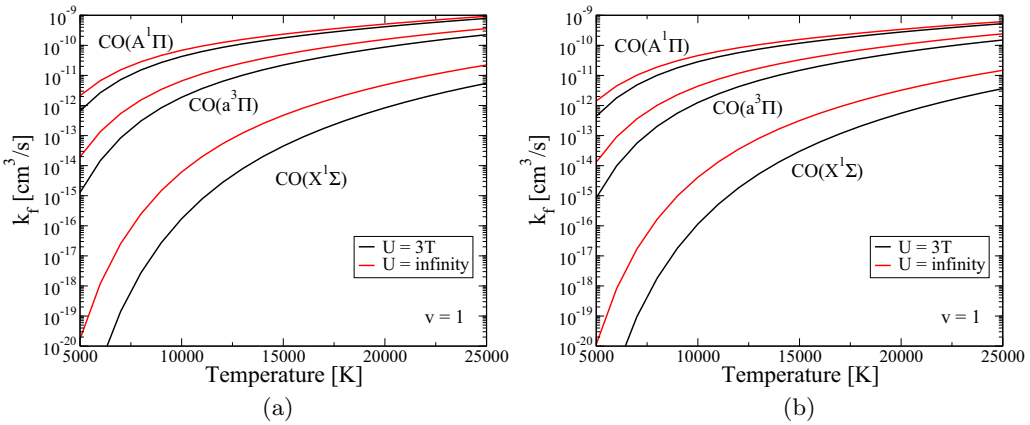

FIG. 2. Dissociation rate coefficients (k_{CO}^f) from different electronic levels. Curves correspond to the electronic states X $^1\Sigma^+$, a $^3\Pi$, and A $^1\Pi$. (a) Collisions with C, N, and O. (b) Collisions with all other heavy partners.

right-hand-side vector **b** are

$$\mathbf{A}_{1i} = \frac{g_i}{\tilde{Q}^{\mathrm{el}}(T_{\mathrm{ve}})} \exp\left(-\frac{E_i}{\mathrm{k_B} T_{\mathrm{ve}}}\right), \tag{15}$$

$$\mathbf{A}_{ii} = \sum_{\substack{j\neq i \\ j\in\mathcal{E}}} k_{ij}^{\mathrm{Exe}}(T_{\mathrm{ve}}) + \sum_{m\in\mathcal{S}_{\mathrm{h}}} \sum_{\substack{j\neq i \\ j\in\mathcal{E}}} \frac{n_m}{n_{\mathrm{e}}} k_{ij(m)}^{\mathrm{Exh}}(T_{\mathrm{ve}}) + \sum_{m\in\mathcal{S}_{\mathrm{h}}} \frac{n_m}{n_{\mathrm{e}}} k_{i(m)}^{\mathrm{D}}(T_{\mathrm{ve}}), \quad i > 1, \tag{16}$$

$$\mathbf{A}_{ij} = -k_{ij}^{\mathrm{Exe}}(T_{\mathrm{ve}}) - \sum_{m\in\mathcal{S}_{\mathrm{h}}} \frac{n_m}{n_{\mathrm{e}}} k_{ij(m)}^{\mathrm{Exh}}(T_{\mathrm{ve}}), \quad i > 1, \quad i \neq j, \tag{17}$$

$$\mathbf{b}_1 = n_{\mathrm{CO}} \Big/ \sum_{i\in\mathcal{E}} n_i^{\mathrm{I}}, \tag{18}$$

$$\mathbf{b}_i = \sum_{m\in\mathcal{S}_{\mathrm{h}}} \frac{n_m}{n_{\mathrm{e}}} \frac{n_i^{\mathrm{D}}}{n_i^{\mathrm{I}}} k_{i(m)}^{\mathrm{D}}(T_{\mathrm{ve}}), \quad i \neq 1, \tag{19}$$

where $i, j \in \mathcal{E}$. It is important to mention that the potential nonlinearities that may arise due to the inclusion of kinetic processes involving different energy levels of CO are eliminated since (1) the elementary reaction rate coefficients do not depend on the excitation of the collision partner and (2) the total CO number density is known.

2. *Multitemperature model*

Rate coefficients. For the kinetic processes treated in a MT manner (e.g., dissociation of N_2), the endothermic rate coefficients are evaluated based on the modified Arrhenius' law [Eq. (14)]. The fitting coefficients can be found in work of Johnston *et al.* [27]. The activation temperature depends on the reaction type (e.g., for dissociation by heavy-particle impact, $T_{\mathrm{a}} = \sqrt{T T_{\mathrm{ve}}}$). Exothermic rate coefficients are computed, as in Sec. II B 1, based on detailed balance.

Energy transfer terms. The energy transfer terms account for the energy losses due to (1) excitation and ionization by electron impact reactions, (2) vibrational-translational energy transfer, (3) production or destruction of heavy-particle vibrational-electronic energy in chemical reactions, and (4) elastic collisions between free-electrons and heavy particles.

At large speeds, it is important to account for electron energy losses due to ionization of atoms and molecules. If this term is neglected, the kinetic energy loss of the electrons is ignored, resulting in a large number of high-energy electrons being produced. This can result in massive ionization rates and thus numerical instabilities. The volumetric free-electron energy loss rates due to ionization (Ω^{I}) and excitation (Ω^{E}) reactions are

$$\Omega^{\mathrm{I}} = \sum_{r\in\mathcal{R}^{\mathrm{I}}} \omega_{\mathrm{e}}^r \mathcal{U}^r, \quad \Omega^{\mathrm{E}} = \sum_{r\in\mathcal{R}^{\mathrm{E}}} \omega_{\mathrm{e}}^r \mathcal{U}^r, \tag{20}$$

where quantities $\mathcal{U}^r$ and ω_{e}^r denote, respectively, the reaction enthalpy and the free-electron mass production rate in reaction r. The sets $\mathcal{R}^{\mathrm{I}}$ and $\mathcal{R}^{\mathrm{E}}$ store, respectively, the electron impact ionization and excitation reactions.

The volumetric time rate of change of vibrational energy due to vibrational-translational energy transfer (Ω^{VT}) is modeled based the Landau-Teller formula:

$$\Omega^{\mathrm{VT}} = \sum_{m\in\mathcal{S}_{\mathrm{m}}} n_m \frac{\tilde{E}_m^{\mathrm{v}}(T) - \tilde{E}_m^{\mathrm{v}}(T_{\mathrm{ve}})}{\tau_m^{\mathrm{VT}}(T)}. \tag{21}$$

The average relaxation time for molecule m is computed as $\tau_m^{\mathrm{VT}} = n_{\mathrm{h}} / \sum_{s\in\mathcal{S}_{\mathrm{h}}} (n_s/\tau_{ms}^{\mathrm{VT}})$, where the elementary relaxation times τ_{ms}^{VT} are evaluated based on Millikan-White's formula including Park's high-temperature correction [13,64].

The volumetric rate of change of vibrational and electronic energy of heavy particles due to chemical reactions is computed according to the nonpreferential dissociation model proposed by

Candler [65]:

$$\Omega^{\mathrm{CV}} = \sum_{s\in\mathcal{S}_{\mathrm{m}}} \omega_s\, \tilde{E}_s^{\mathrm{v}}(T_{\mathrm{ve}})/m_s, \quad \Omega^{\mathrm{CE}} = \sum_{s\in\mathcal{S}_{\mathrm{h}}^*} \omega_s\, \tilde{E}_s^{\mathrm{el}}(T_{\mathrm{ve}})/m_s, \tag{22}$$

where quantity ω_s denotes the mass production rate of species s due to all reactions. Note that the electronic states of CO are not taken into account in the evaluation of Ω^{CE}.

The volumetric free-electron energy loss rate due to elastic collisions with heavy particles is

$$\Omega^{\mathrm{ET}} = 3n_{\mathrm{e}}\, \mathrm{k_B}\, \nu_{\mathrm{e}}^{\mathrm{ET}}(T - T_{\mathrm{ve}}), \tag{23}$$

where the energy exchange collision frequency is obtained based on the Kinetic Theory of Gases, $\nu_{\mathrm{e}}^{\mathrm{ET}} = \sum_{s\in\mathcal{S}_{\mathrm{h}}}(m_{\mathrm{e}}/m_s)\nu_{es}$ [66,67]. The collision frequencies for the individual electron-heavy interactions are evaluated as $\nu_{es} = n_s\, \Omega_{es}^{(1,1)} \sqrt{8\mathrm{k_B}T_{\mathrm{ve}}/\pi m_{\mathrm{e}}}$, where quantities $\Omega_{es}^{(1,1)}$ are the electron-heavy collision integrals in the first-order Sonine-Laguerre polynomial expansion.

C. Radiative processes

In this section we briefly discuss the formulation of the monochromatic emission, η_λ, and absorption, κ_λ, coefficients for the bound-bound radiative processes for nonequilibrium plasmas, assuming a StS formulation. These coefficients are necessary to the determination of the radiative signature of the gas.

When considering molecular systems, all the transitions characterized by absorption and emission of light are subdivided into three types: free-free transitions, bound-free transitions, and bound-bound transitions. The present analysis is carried out considering only the bound-bound radiation, which is the result of *rovibronic* transitions among bound molecular states. This type of radiation is also referred to as line radiation, owing to its discrete nature. When modeling line radiation, three mechanisms have to be considered: spontaneous emission, absorption, and stimulated emission. These processes require the knowledge of one of the three transition probabilities also known as Einstein coefficients for spontaneous or induced emission (A_{ul} and B_{ul}, respectively, where u and l denote, respectively, the upper and the lower rovibronic states in the transition) and absorption B_{lu}. The Einstein coefficients used in this work are part of the HYPER-RAD database. HYPER-RAD is being developed at NASA Ames Research Center and comprises a list of transition probabilities, energy levels, and line positions. *Ab initio* calculations are used for electric dipole and quadrupole, magnetic dipole, and spin-forbidden transitions, which include fine structure, predissociation, and nonadiabatic corrections. More details regarding the development of the HYPER-RAD database are given in Ref. [5].

The knowledge of transition probabilities allows for the determination of the monochromatic emission and absorption coefficients:

$$\eta_\lambda = \sum_{ul} n_u \frac{A_{ul}}{4\pi} \frac{\mathrm{h_P}c}{\lambda_{ul}} \phi(\lambda - \lambda_{ul}), \quad \kappa_\lambda = \sum_{ul} (n_l B_{lu} - n_u B_{ul}) \frac{\mathrm{h_P}}{\lambda_{ul}} \phi(\lambda - \lambda_{ul}), \tag{24}$$

where λ stands for the wavelength. Quantities c and λ_{ul} stand for the speed of light and the transition wavelength, respectively. The symbol $\phi(\lambda - \lambda_{ul})$ denotes the line-shape function. In this work, a Voigt profile is adopted to account for Doppler, collisional, and Stark broadening. Doppler and collisional broadening are computed at T, while the vibronic temperature $\mathrm{T_{ve}}$ is used for Stark broadening. In order to speed up the calculation, the integral defining the Voigt function is approximated by means of the fitting formula proposed by Whiting [68]. The populations of the upper and lower rovibronic states to be used in the computation of the emission and absorption coefficients [Eq. (24)] are obtained based on a Boltzmann distribution for the rovibrational population of each electronic state:

$$\frac{n_{(i,v,J)}}{n_i} = \frac{g_J}{\tilde{Q}_i^{\mathrm{rv}}(T_{\mathrm{r}}, T_{\mathrm{ve}})} \exp\left(-\frac{E_{(i,v,J)}^{\mathrm{r}}}{\mathrm{k_B}T_{\mathrm{r}}} - \frac{E_{(i,v)}^{\mathrm{v}}}{\mathrm{k_B}T_{\mathrm{ve}}}\right), \tag{25}$$

where the population of the electronic states, n_i, are obtained by using either the StS or the QSS approach. Due to the assumed rotational equilibrium, $T_\mathrm{r} = T$ in Eq. (25). In the former equation, quantities g_J, $E^\mathrm{r}_{(i,v,J)}$ and $E^\mathrm{v}_{(i,v)}$ denote, respectively, the degeneracy of the Jth rotational state and the rotational and vibrational energies of the rovibronic state (i,v,J). The symbol $\tilde{Q}^\mathrm{rv}_i(T_\mathrm{r},T_\mathrm{ve})$ stands for the multitemperature rovibrational partition function of the electronic state i. In the case of the MT model (when one solves for the global number density of CO), Eq. (25) has to be be replaced by

$$\frac{n_{(i,v,J)}}{n_\mathrm{CO}} = \frac{g_J\, g_i}{\tilde{Q}^\mathrm{rve}(T_\mathrm{r},T_\mathrm{ve},T_\mathrm{ve})} \exp\left(-\frac{E^\mathrm{r}_{(i,v,J)}}{\mathrm{k_B} T_\mathrm{r}} - \frac{E^\mathrm{v}_{(i,v)}}{\mathrm{k_B} T_\mathrm{ve}} - \frac{E_i}{\mathrm{k_B} T_\mathrm{ve}}\right), \tag{26}$$

where quantity $\tilde{Q}^\mathrm{rve}(T_\mathrm{r},T_\mathrm{ve},T_\mathrm{ve}) = \sum_{i\in\mathcal{E}} g_i \exp(-E_i/\mathrm{k_B}T_\mathrm{ve})\, \tilde{Q}^\mathrm{rv}_i(T_\mathrm{r},T_\mathrm{ve})$ is the multitemperature rovibronic (i.e., internal) partition function of CO.

D. Flow governing equations

The inviscid nonequilibrium flow behind a normal shock wave is studied using either the MT approach or the STS model developed in Secs. II B 1 and II B 2. The MT model is the two-temperature model developed by Park in Refs. [4,12,13]. This model assumes thermal equilibrium between translational and rotational energy modes, and the remaining modes (vibrational, electronic, and free electrons) are out of equilibrium and have the common temperature T_{ve}. In addition, any coupling effects between the flow and radiation are neglected by using an escape factor equal to zero.

Both physico-chemical models have been implemented in a one-dimensional flow solver, SHOCKING [32,38]. This tool computes the flow behind a normal shock wave by solving (in the shock reference frame) the Euler equations, which comprise the species continuity equations, the global momentum, and global energy equations:

$$\frac{\partial}{\partial x}\begin{pmatrix} \rho_s u \\ p + \rho u^2 \\ \rho u H \end{pmatrix} = \begin{pmatrix} \omega_s \\ 0 \\ 0 \end{pmatrix}, \tag{27}$$

$s \in \mathcal{S}$, where the partial densities are defined as $\rho_s = n_s m_s$. Quantity ρH denotes the gas total enthalpy density, $\rho H = \rho e + p + \rho u^2/2$, where u is the flow velocity. To close the system, one must add to Eq. (27) an additional energy equation for the vibrational, electronic, and free-electron energy modes in equilibrium at T_ve:

$$\frac{\partial}{\partial x}\left[\left(\rho e_\mathrm{e} + \rho e_\mathrm{elv} - \sum_{i\in\mathcal{E}} n_i E_i\right)u\right] = -p_\mathrm{e}\frac{\partial u}{\partial x} + \Omega^\mathrm{CV} + \Omega^\mathrm{CE} + \Omega^\mathrm{VT} + \Omega^\mathrm{ET} - \Omega^\mathrm{I} - \Omega^\mathrm{E}. \tag{28}$$

Note that the energy content associated to the CO electronic states, $\sum_{i\in\mathcal{E}} n_i E_i$, is subtracted from the gas vibrational-electronic-free-electron energy density, $\rho e_\mathrm{e} + \rho e_\mathrm{elv}$, due to the use of a StS approach. In the MT formulation, the source term due electron impact excitation Ω^E drops out, and Eq. (28) modifies according to

$$\frac{\partial}{\partial x}\left[\left(\rho e_\mathrm{e} + \rho e_\mathrm{elv}\right)u\right] = -p_\mathrm{e}\frac{\partial u}{\partial x} + \Omega^\mathrm{CV} + \Omega^\mathrm{CE} + \Omega^\mathrm{VT} + \Omega^\mathrm{ET} - \Omega^\mathrm{I}. \tag{29}$$

The initial condition needed to solve Eqs. (27) and (28) is obtained based on the Rankine-Hugoniot jump relations. In applying this procedure, the gas composition and the temperature of the nonequilibrium energy modes (e.g., vibrational, electronic) are assumed to be frozen to their free-stream values. Equations (27) and (28) are numerically integrated by using the family of Backward-Differentiation-Formula methods [69] as implemented in the LSODE FORTRAN library [70].

E. Radiation transport

A line-by-line radiation code, HPC-RAD, is employed to calculate the radiation intensity in the shock-heated plasma based on the converged shock-layer thermo-chemistry. The radiation model is decoupled from the flow solver mentioned above; i.e., the flow is not influenced by radiation effects (e.g., radiative cooling).

The radiative signature of the gas is governed by the radiative transfer equation (RTE). For steady-state radiation and one-dimensional geometries, the former equation reads [71]

$$\mu \frac{\partial I_{\lambda\mu}}{\partial x} = \eta_\lambda - \kappa_\lambda I_{\lambda\mu}, \tag{30}$$

where quantity $I_{\lambda\mu}$ is the monochromatic intensity along the direction μ. The symbol μ denotes the cosine of the angle (θ) between the x axis and the line of sight (i.e., $\mu = \cos\theta$). The monochromatic emission and absorption coefficients are computed as explained in Sec. II C. In this work, the radiation and flow solver are not coupled, and radiation is computed from the flow field, without considering radiative terms in the species continuity and energy equations.

In order to enable future comparisons with the experimental results acquired in the EAST facility, the RTE (30) is solved along the tube radius, (i.e., $\mu = 1$) by assuming a homogeneous medium [72]. Under these conditions, the RTE can be integrated exactly to obtain the monochromatic intensity at the wall location:

$$I_\lambda(D) = S_\lambda\,[1 - \exp(-\kappa_\lambda\, D)], \tag{31}$$

where the monochromatic source function is $S_\lambda = \eta_\lambda/\kappa_\lambda$. Quantity D denotes the tube diameter.

The radiative heat-flux along the flow direction is evaluated as

$$q_\lambda(x) = 2\pi \int_{-1}^{1} I_{\lambda\mu}(x)\mu\, d\mu, \tag{32}$$

where the directions $\mu = 1$ and $\mu = -1$ correspond now to a line of sight parallel and antiparallel to the x axis, respectively. The directional dependent monochromatic intensity $I_{\lambda\mu}$ is obtained, as before, by integrating analytically Eq. (30) under the assumption of a homogeneous medium (i.e., tangent slab method) [71]. Finally, the spectrally integrated heat flux is computed by integrating Eq. (32) over the wavelength range of the CO fourth positive system:

$$q(L) = \int_{\lambda_1}^{\lambda_2} q_\lambda(L)\, d\lambda, \tag{33}$$

where the lower and upper bounds of the integral are $\lambda_1 = 165\,\text{nm}$ and $\lambda_2 = 195\,\text{nm}$, respectively. Quantity L denotes the thickness of the shock layer.

III. RESULTS

The StS and QSS nonequilibrium models, describing the detailed kinetics behind a normal shock, are applied to the study of nonequilibrium radiation for a wide range of conditions. The observables calculated and discussed are radiation signature in direction perpendicular to the axis of the shock tube, integrated heat flux in direction of the tube axis, population distribution of the electronic energy levels of CO, and temperature profiles.

The analysis of the results is organized as follows. The validity of the QSS assumption is investigated in Sec. III A. In the same section, the influence of dissociation on the radiative signature is also discussed. Section III B investigates the influence of different *activation* temperature when building up a self-consistent QSS model.

TABLE III. Shock-tube flow characteristic quantities.

	Free-stream	Postshock
Pressure [Pa]	1.0	927.15
Velocity [km/s]	8.0	1.342
Temperature [K]	300.0	46649.3
X_{CO_2}	0.96	0.96
X_{N_2}	0.04	0.04

A. Assessment of the validity of the QSS assumption

In this section the collisional-radiative model previously described is applied to the study of atmospheric entry of Pathfinder into Mars atmosphere. During this entry a significant portion of the overall wall heat flux was due to radiation. Most of the radiation (approximately 70%) came from CO fourth positive, and thus an accurate prediction of the populations of excited electronic states of the CO molecules is crucial.

Most of the analyses of the radiation heating carried out at a Mars entry condition have been conducted by using the QSS assumption [8,27]. However, the validity of this assumption has not been verified. Thus, the focus of this section is the assessment of the existence of a quasistationary distribution between the electronic states of CO molecules for free-stream velocities ranging between 6 and 8 km/s and free-stream pressures between 1 and 100 Pa. The results analyzed here correspond to the conditions shown in Table III. Additional test cases can be found in the Supplemental Material [50].

The characterization of the thermodynamic state of the plasma in the shock layer requires the knowledge of its chemical composition as well as the internal energies of the particles. To this aim Fig. 3 shows the evolution of the rotational or translational temperature and the vibrational or free-electron temperature. After a jump in the translational temperature across the shock (located on the left at $x = 0$), the gas redistributes energy through excitation of the internal energy modes as well as the onset of chemical reactions, until the flow eventually reaches its postshock equilibrium state.

Figure 3(a) compares temperature profiles obtained with MT and StS methods. The temperatures evolution is qualitatively similar for the two models throughout the entire computational domain. The StS model seems to predict a slower relaxation and in general larger translational and vibrational temperatures between 3 and 6 cm behind the shock. However, the analysis of the CO number density in Fig. 3(b) shows differences in the prediction of the number density of the excited states, between the two models, and particularly in correspondence of their peak values. The QSS model predicts faster

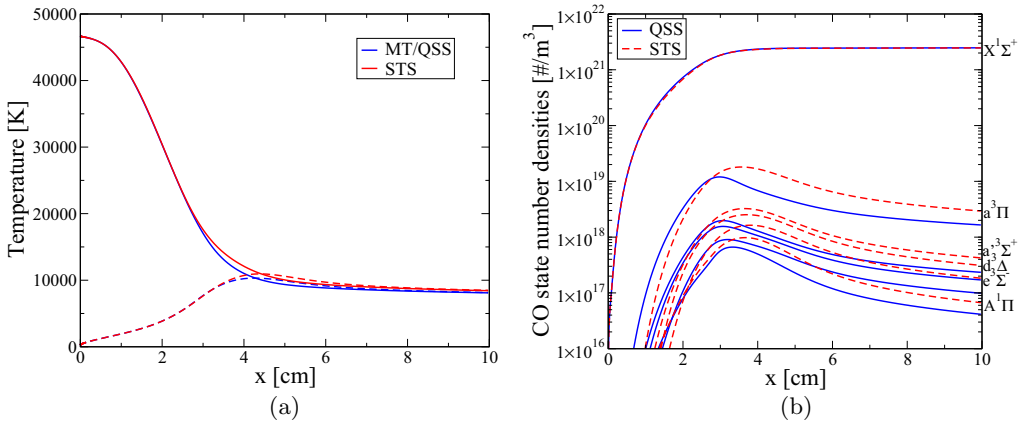

FIG. 3. Comparison between QSS and StS models using state-specific dissociation. (a) Temperature distribution. (b) CO state populations.

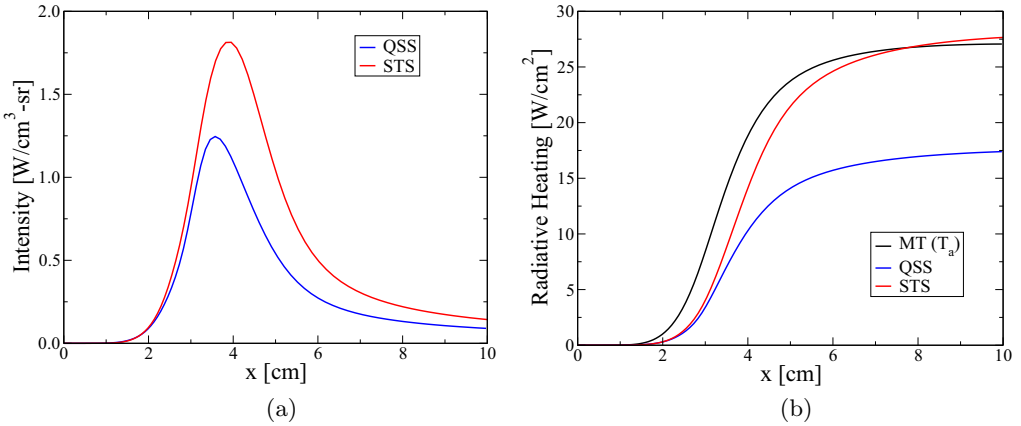

FIG. 4. Comparison between QSS and StS model radiation quantities using state-specific dissociation for $\lambda \in (165,195)$ nm. (a) Spectrally integrated intensity. (b) Spectrally integrated radiative heat flux.

relaxation and dissociation. It is important to note that since the QSS model is decoupled from the flow calculation the dissociation predicted by the QSS cannot influence the total CO concentration of the flow field and ultimately is responsible for the differences in the population of the excited states. Because radiation is directly related to the population of the electronic states of CO for optically thin gases, this will translate into significant differences in the radiation signatures predicted.

Figure 4 shows the spectrally integrated intensity ($\lambda \in [165,195]$ nm) in direction perpendicular to the shock-tube axis and heat flux in the flow direction. The QSS model underpredicts the radiative intensity nonequilibrium overshoot seen in the StS model by as much as 45%. Differences between the StS and QSS models are observed in correspondence of the peak intensity and in the relaxation to equilibrium. This behavior has been observed over a wide range of entry conditions. At lower free-stream velocities, since dissociation of CO is drastically reduced, the two model predictions are in good agreement. The comparison of the heat-flux profiles allows for the discrepancies on the radiation heating to be quantified. For a standoff distance of 10 cm, the StS model predicts 57.6% larger heating, thus invalidating the QSS assumption.

The knowledge of the electronic level population allows for the determination of the electronic temperature of CO molecules $T_{e,\mathrm{CO}}$. There are different ways to extract a temperature from a given distribution, in this analysis $T_{e,\mathrm{CO}}$ was computed electronic energy by solving the following equation:

$$\frac{\sum_{i\in\mathcal{E}} n_i E_i}{n_{\mathrm{CO}}} = \frac{\sum_{i\in\mathcal{E}} g_i E_i \exp\left(-\frac{E_i}{k_B T_{\mathrm{ve}}}\right)}{\tilde{Q}^{\mathrm{el}}(T_{\mathrm{ve}})}. \tag{34}$$

Figure 5 shows $T_{e,\mathrm{CO}}$, T, T_{ve}, and $T_a = \sqrt{T T_v}$ as predicted using the QSS and STS models. Contrary to what assumed by the MT models, the electronic temperature of CO is much closer to T_a than to T_v, owning to the dominant contribution of the heavy particle driven processes to the excitation of the electronic energy levels. Thus, the conventional assumption T_e=T_{ve} is invalid, when heavy particle processes dominate the excitation of the electronic energy. This is not the case for higher speeds where the electronic excitation is controlled by electrons [12]. The similarities in the evolution of $T_{e,\mathrm{CO}}$ and T_a justify the similarities in the prediction of the radiative heating between the StS model and the MT model shown in Fig. 4. In this MT case, the radiation was computed assuming that CO($A^1\Pi$) is populated according to a Maxwell-Boltzmann distribution at T_{a}.

In Fig. 6 the population of the excited level is shown in correspondence of the nonequilibrium overshoot, where the differences between the QSS and MT models are more pronounced. The distribution of the electronic levels can be closely represented by a Maxwell-Boltzmann at $T_{\mathrm{ve}} < T_{e,\mathrm{CO}} < T_a$. Strong deviations from Boltzmann distribution are observed for the CO($A^1\Pi$).

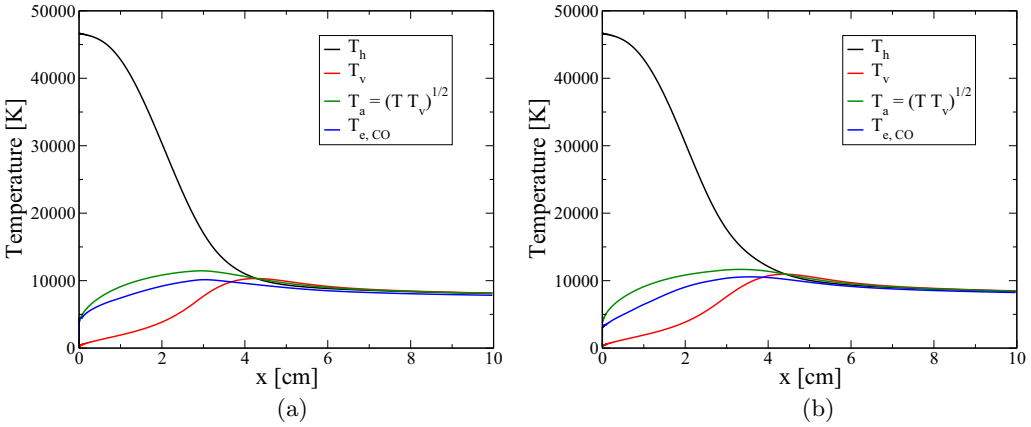

FIG. 5. Temperature distribution computed from QSS and StS model using state-specific dissociation. (a) Using QSS model. (b) Using StS model.

The overpopulation of this state is due to the large excitation rate coefficient for the $(X^1\Sigma^+ - A^1\Pi)$ collisional processes. In this work the rates describing the collisional excitation from the ground to the $A^1\Pi$ state of CO are taken by Schofield [29], while data from remaining processes are due to Park [60]. The differences in magnitude among these processes is not surprising, since rate coefficients due to heavy particles collisions are large for optically allowed transitions [60].

The primary reason for the disagreement between the QSS and StS models is because the effect of dissociation from the excited states is not properly captured by the MT/QSS model. The results in Fig. 7 show the spectrally integrated intensity and radiative heat flux when the dissociation from the excited states has been hindered and only ground state dissociation has been included in the calculation. The predictions of StS and MT are in excellent agreement, confirming the importance of a tighter coupling between electronic state kinetics and flow calculation when dissociation is significant. However, the heating rates are 20% lower than what is predicted using the STS model with state-specific dissociation (Fig. 7).

Figure 8 shows the value of the radiative heating, assuming 10 cm standoff distance, for different values of the free stream pressure, as predicted by the QSS and StS model. This allows for the assessment of the validity of QSS assumption, and more importantly it allows one to quantify its impact on the radiative heating. Two different shock velocities are considered: 7 km/s [Fig. 8(a)] and

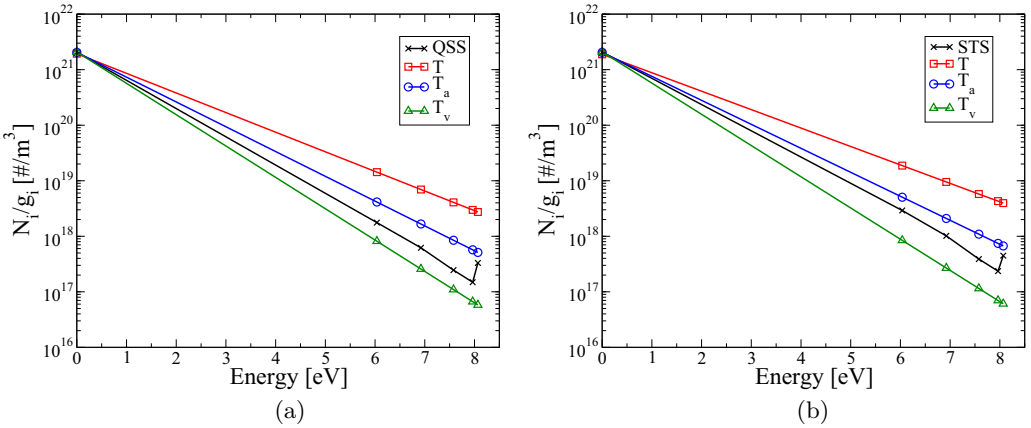

FIG. 6. State populations and corresponding Boltzmann distributions at the various flow temperatures at the nonequilibrium overshoot location. (a) From QSS solution. (b) From StS solution.

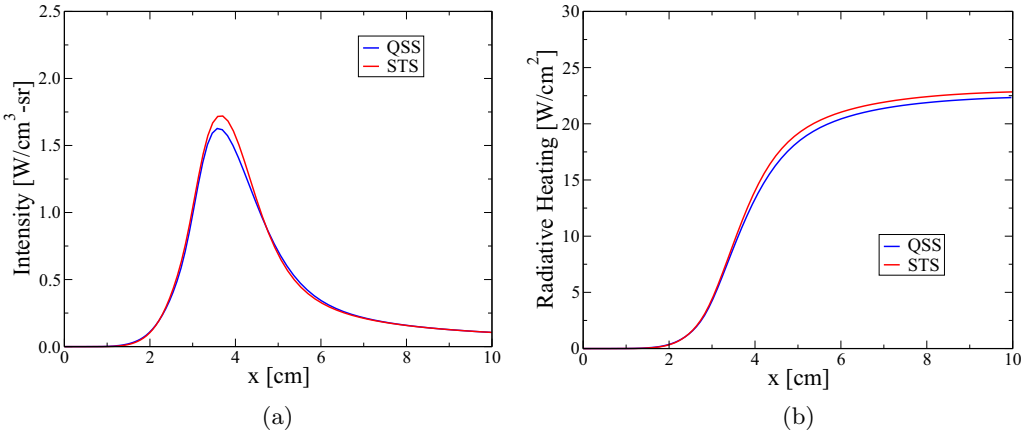

FIG. 7. Comparison between QSS and StS model radiation quantities using ground state dissociation for $\lambda \in (165, 195)$ nm. (a) Spectrally integrated intensity. (b) Spectrally integrated radiative heat flux.

8 km/s [Fig. 8(b)]. In both cases the QSS model underpredicts the heating rates when compared to the STS model: in the 8 km/s case the maximum difference is as much as 50%, while the difference is about 25% at 7 km/s.

The nonmonotonic behavior of the heat-flux curves shown in Fig. 8 can be explained as follows: at low pressures the nonequilibrium effects cause an overshoot in the radiation flux caused by the excess of CO in the gas. As pressure increases the overshoot disappears and the radiation output is reduced. At higher pressure, however, although nonequilibrium effects become less important, radiation increases because of the increase in the postshock densities and pressures.

B. Self-consistent QSS model

In MT models the distribution of the electronic energy levels of the gas particles is described by the Maxwell-Boltzmann equation. This section discusses the implications of using a physically consistent Boltzmann weighting to describe dissociation of CO molecules.

When averaged over a Maxwell-Boltzmann distribution the rates in Table II yield the global dissociation rate coefficient, $k^{\mathrm{D}}_{(m)}$, given by Johnston [27]. The expression for the averaged rate

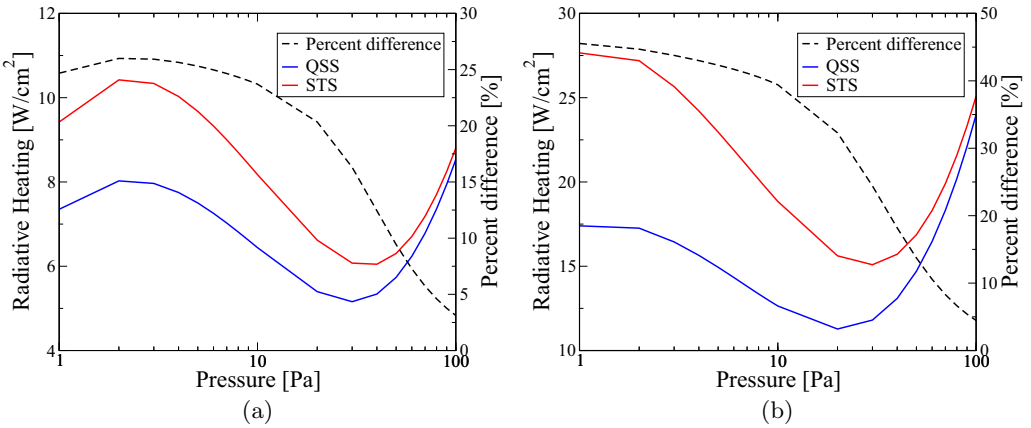

FIG. 8. Radiative heat flux [$\lambda \in (165, 195)$ nm] at 10 cm past the shock wave as predicted by QSS and StS models. (a) Free-stream velocity 7 km/s. (b) Free-stream velocity 8 km/s.

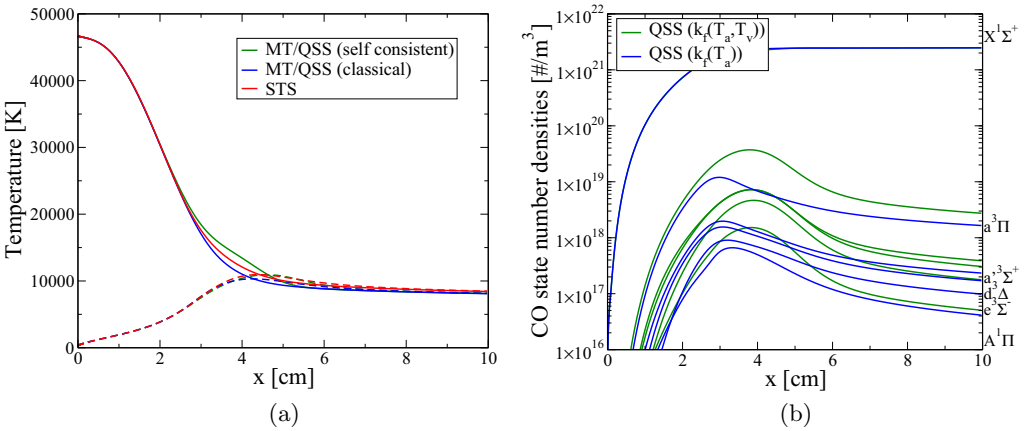

FIG. 9. Comparison between QSS and StS model using state-specific dissociation in the self-consistent and conventional QSS method. (a) Temperature profiles. (b) CO state populations.

coefficient is

$$k^{\mathrm{D}}_{(m)} = \frac{1}{\tilde{Q}^{\mathrm{el}}(T_{\mathrm{ve}})} \sum_{i\in\mathcal{E}} g_i \, k^{\mathrm{D}}_{i(m)}(T_{\mathrm{a}}) \exp\left(-\frac{E_i}{\mathrm{k_B} T^\star}\right), \tag{35}$$

where $T^\star$ is the temperature governing the excitation of the molecular electronic states. In MT models the use of $k^{\mathrm{D}}_{(m)}$ at T_a implies the use of T_a (i.e., $T^\star = T_a$) in the Boltzmann weight in Eq. (35). Since the MT models assume a Boltzmann population distribution at T_v, to be physically consistent with the model $T^\star$ should be evaluated at T_v.

Figure 9 shows the temperature and population density profiles for the Pathfinder case previously discussed. The comparison of temperature and densities profiles with the results shown in Sec. III A reveals a significant reduction of the CO dissociation rates for the electronically excited states of CO. This is not surprising since T_{ve} is bound to be lower than T_{a} in shock-heated flows. The lower degree of dissociation explains the increase of translational temperatures in the shock layer between 3 and 6 cm.

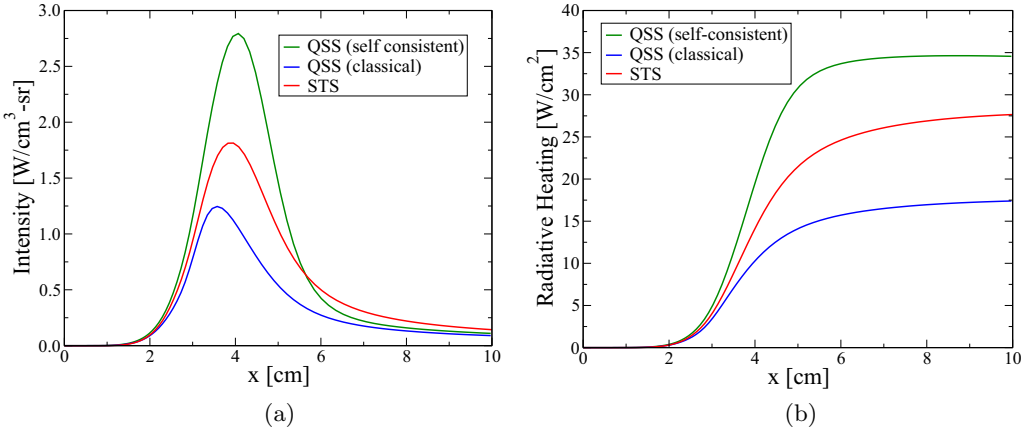

FIG. 10. Comparison between StS, conventional and self-consistent QSS models radiation quantities using state-specific dissociation for $\lambda \in (165, 195)$ nm. (a) Spectrally integrated intensity. (b) Spectrally integrated radiative heat flux.

Figure 10 shows the radiation properties calculated using the consistent QSS approach. By slowing dissociation, the CO number density is increased and the radiation is significantly enhanced. Both the peak intensity and radiative heating from the two QSS models straddle the STS model, with the previous form under predicting and the latter QSS over predicting.

IV. SUMMARY AND DISCUSSION

We have performed an in-depth analysis of the nonequilibrium radiation generated by hot CO_2-N_2 gas mixtures produced by a strong normal shock. We have studied the departure of the electronic energy populations of CO molecules from the Maxwell-Boltzmann distribution at conditions relevant to Mars entry applications. Two different approaches have been considered: (1) StS approach, where the state master equations are solved together with the flow-governing equation in a tightly coupled manner; (2) QSS approach, where a system of algebraic equations is used to compute the population of the electronically excited states of CO. A MT model was used to supply the CO number densities and temperatures to the QSS model that was run in the postprocessing phase, when computing the radiation properties of the gas.

The kinetic model used was previously developed by Johnston *et al.* [27]. The modifications were introduced to account for the dissociation from the excited electronic states of CO. In order to model dissociation from these states, we have used the method developed by Aliat *et al.* [31], which allows for the scaling of the global dissociation rate extracted by Johnston and based on recent experimental data collected on the EAST shock tube.

It was found that the population of the excited states of CO molecules can be closely represented by a Maxwell-Boltzmann distribution, with the exception of the $CO(A^1\Pi)$ state, which is significantly overpopulated. This is due to the large excitation rate coefficients for the $CO(X^1\Sigma^+\text{-}A^1\Pi)$ transition used in our calculations.

The comparison of the results obtained with the QSS models against the more physically consistent StS approach revealed the invalidity of the QSS assumption. This assumption, commonly used in nonequilibrium flows, fails in presence of significant dissociation, for entry velocities ranging from 7 to 8 km/s. At lower velocities the dissociation is strongly reduced, and the QSS and STS predictions are in closer agreement.

In order to assess the impact of the QSS assumption on the prediction of radiative heating for Mars entry application a parametric study of the radiation heating for free-stream velocities ranging from 7 to 8 km/s and free-stream pressure ranging from 1 to 100 Pa has been performed. It was found that the approximation used to describe nonequilibrium effects have a significant impact on the prediction of radiation heating, with the QSS models underpredicting radiation heat loads by as much as 50% at a speed of 8 km/s and 25% at a speed of 7 km/s.

ACKNOWLEDGMENTS

Support from the NASA Entry System Modeling Project in the Space Technology Mission Directory is gratefully acknowledged. Program Managers are Dr. M. Wright and Dr. M. Barnhardt at NASA Ames Research Center, under Grant No. NNX14AB67A. The authors would like to thank the NASA Ames quantum computational chemistry group (in particular Dr. D. W. Schwenke and Dr. R. L. Jaffe) for sharing the Hyper-rad database.

[1] P. A. Gnoffo, Planetary-entry gas dynamics, Annu. Rev. Fluid Mech. **31**, 459 (1999).

[2] C. O. Johnston, Influence of radiative absorption on non-Boltzmann modeling for Mars entry, J. Thermophys. Heat Transfer **28**, 795 (2014).

[3] S. T. Surzhikov, Radiation gas dynamics of Martian space vehicles, Doklady Phys. **57**, 119 (2012).

[4] C. Park, J. T. Howe, and R. L. Jaffe, Review of chemical-kinetic problems of future NASA missions, II: Mars entries, J. Thermophys. Transfer **8**, 9 (1994).
[5] A. M. Brandis, C. O. Johnston, B. M. Cruden, and D. Prabhu, Investigation of nonequilibrium radiation for Mars entry, AIAA paper 2013-1055, 51st AIAA Aerospace Sciences Meeting including the New Horizons Forum and Aerospace Exposition, Aerospace Sciences Meetings, Grapevine (Dallas/Ft. Worth Region), TX, 7–10 January, 2013.
[6] J. O. Arnold, V. H. Reis, and H. T. Woodward, Studies of shock-layer radiation of bodies entering planetary atmospheres, AIAA J. **3**, 2019 (1965).
[7] J. Nealy, An experimental study of ultraviolet radiation behind incident normal shock waves in CO_2 at Venusian entry speeds, AIAA/AGU Conference on the Exploration of the Outer Planets, AIAA paper 1975-1150, St. Louis, MO, 17–19 September, 1975.
[8] C. O. Johnston, A. M. Brandis, and K. Sutton, Shock layer radiation modeling and uncertainty for Mars entry, AIAA paper 2012-2886, 43rd AIAA Thermophysics Conference, Fluid Dynamics and Co-located Conferences, New Orleans, LA, 25–28 June, 2012.
[9] A. M. Brandis, C. O. Johnston, B. A. Cruden, D. K. Prabhu, A. A. Wray, Y. Liu, D. W. Schwenke, and D. Bose, Validation of CO 4th positive radiation for Mars entry, J. Quant. Spectrosc. Radiat. Transfer **121**, 91 (2013).
[10] J. T. Howe, J. R. Viegas, and Y. S. Sheaffer, Study of the non-equilibrium flow field behind normal shock waves in carbon dioxide, NASA Technical Paper TN D-1885 (1963).
[11] G. Candler, Computation of thermo-chemical nonequilibrium Martian atmospheric entry flows, AIAA paper 1990-1695, AIAA/ASME 5th Joint Thermophysics and Heat Transfer Conference, Seattle, WA, 18–20 June, 1990.
[12] C. Park, *Nonequilibrium Hypersonic Aerothermodynamics* (John Wiley and Sons, New York, 1990).
[13] C. Park, Review of chemical-kinetic problems of future NASA missions, I: Earth entries, J. Thermophys. Heat Transfer **7**, 385 (1993).
[14] I. Armenise and E. V. Kustova, State-to-state models for CO_2 molecules: From the theory to an application to hypersonic boundary layers, Chem. Phys. **415**, 269 (2013).
[15] I. Armenise and E. V. Kustova, On different contributions to the heat flux and diffusion in nonequilibrium flows, Chem. Phys. **428**, 90 (2014).
[16] V. A. Gorelov, M. K. Gladyshev, A. Y. Kireev, and S. V. Shilenkov, Nonequilibrium ionization behind a strong shock wave in the Mars atmosphere, J. Appl. Mech. Tech. Phys. **41**, 970 (2000).
[17] N. Kudryavtsev, L. Kuznetsova, and S. Surzhikov, Kinetics and nonequilibrium radiation of CO_2-N_2 shock waves, in *32nd AIAA Plasmadynamics and Lasers Conference, Fluid Dynamics and Co-located Conferences, Anaheim, CA, 11-14 June 2001* (AIAA, 2001), paper 2001-2728.
[18] A. Aliat, A. Chikhaoui, and E. V. Kustova, Nonequilibrium kinetics of a radiative CO flow behind a shock wave, Phys. Rev. E **68**, 056306 (2003).
[19] E. V. Kustova and E. V. Nagnibeda, On a correct description of a multi-temperature dissociating CO_2 flow, Chem. Phys. **321**, 293 (2006).
[20] E. V. Kustova, E. A. Nagnibeda, L. A. Puzyreva, and A. Chikhaoui, Non-equilibrium vibration-dissociation kinetics and heat transfer in CO_2-N_2 mixtures, European Space Agency (Special Publication) ESA629SP (2006).
[21] S. T. Surzhikov, Electronic excitation in air and carbon dioxide gas, in *Non-Equilibrium Gas Dynamics—From Physical Models to Hypersonic Flights*, Lecture Series (von Karman Institute for Fluid Dynamics, Rhode-Saint-Genèse, 2008).
[22] E. V. Kustova and E. A. Nagnibeda, Kinetic model for multi-temperature flows of reacting carbon dioxide mixture, Chem. Phys. **398**, 111 (2012).
[23] S. Surzhikov, Radiative gas dynamics of large superorbital space vehicle at angle of attack, AIAA paper 2016-0741, 54th AIAA Aerospace Sciences Meeting, San Diego, CA, 4–8 January, 2016.
[24] G. Zalogin, P. Kozlov, L. Kuznetsova, S. Losev, V. Makarov, Yu. Romanenko, and S. Surzhikov, Radiation excited by shock waves in a CO_2-N_2-Ar mixture: Experiment and theory, Tech. Phys. **46**, 654 (2001).
[25] C. Rond, P. Boubert, J.-M. Felio, and A. Chikhaoui, Nonequilibrium radiation behind a strong shock wave in CO_2-N_2, Chem. Phys. **340**, 93 (2007).

[26] E. S. Lee, C. Park, and K. S. Chang, Shock-tube determination of CN formation rate in a CO_2-N_2 mixture, J. Thermophys. Heat Transfer **21**, 50 (2007).
[27] C. O. Johnston and A. M. Brandis, Modeling of nonequilibrium CO fourth-positive and CN violet emission in CO_2-N_2 gases, J. Quant. Spectrosc. Radiat. Transfer **149**, 303 (2014).
[28] D. R. Bates, A. E. Kingston, and R. W. P. McWhirter, Recombination between electrons and atomic ions. I. Optically thin plasmas, Proc. R. Soc. London A **267**, 297 (1962).
[29] K. Schofield, Critically evaluated rate constants for gaseous reactions of several electronically excited species, J. Phys. Chem. Ref. Data **8**, 723 (1979).
[30] C. Park, Rate parameters for electronic excitation of diatomic molecules II. Heavy particle-impact processes, AIAA paper 2008-1446, 46th AIAA Aerospace Sciences Meeting and Exhibit, Reno, NV, 7–10 January, 2008.
[31] A. Aliat, E. Kustova, and A. Chikhaoui, State-to-state dissociation rate coefficients in electronically excited diatomic gases, Chem. Phys. Lett. **390**, 370 (2004).
[32] M. Panesi, T. E. Magin, A. Bourdon, A. Bultel, and O. Chazot, Electronic excitation of atoms and molecules for the FIRE II flight experiment, J. Thermophys. Heat Transfer **25**, 361 (2011).
[33] A. Lemal, C. M. Jacobs, M.-Y. Perrin, C. O. Laux, P. Tran, and E. Raynaud, Air collisional-radiative modeling with heavy-particle impact excitation processes, J. Thermophys. Heat Transfer **30**, 226 (2016).
[34] A. Lemal, C. M. Jacobs, M.-Y. Perrin, C. O. Laux, P. Tran, and E. Raynaud, Prediction of nonequilibrium air plasma radiation behind a shock wave, J. Thermophys. Heat Transfer **30**, 197 (2016).
[35] A. Bultel, B. van Ootegem, A. Bourdon, and P. Vervisch, Influence of Ar_2^+ in an argon collisional-radiative model, Phys. Rev. E **65**, 046406 (2002).
[36] A. Bultel, B. G. Chéron, A. Bourdon, O. Motapon, and I. F. Schneider, Collisional-radiative model in air for earth re-entry problems, Phys. Plasmas **13**, 043502 (2006).
[37] S. T. Surzhikov, Radiation modeling in shock-tubes and entry flows, in *Non-Equilibrium Gas Dynamics: From Physical Models to Hypersonic Flights*, Lecture Series (von Karman Institute for Fluid Dynamics, Rhode-Saint-Genèse, 2008).
[38] M. Panesi, T. E. Magin, A. Bourdon, A. Bultel, and O. Chazot, Fire II flight experiment analysis by means of a collisional-radiative model, J. Thermophys. Heat Transfer **23**, 236 (2009).
[39] A. Munafò, A. Lani, A. Bultel, and M. Panesi, Modeling of non-equilibrium phenomena in expanding flows by means of a collisional-radiative model, Phys. Plasmas **20**, 073501 (2013).
[40] M. Panesi and A. Lani, Collisional radiative coarse-grain model for ionization in air, Phys. Fluids **25**, 057101 (2013).
[41] I. V. Adamovich, S. O. Macheret, J. W. Rich, and C. E. Treanor, Vibrational energy transfer rates using a forced harmonic oscillator model, J. Thermophys. Heat Transfer **12**, 57 (1998).
[42] G. Colonna and M. Capitelli, Self-consistent model of chemical, vibrational, electron kinetics in nozzle expansion, J. Thermophys. Heat Transfer **15**, 308 (2001).
[43] A. Aliat, P. Vedula, and E. Josyula, State-to-state modeling of radiation coupled to vibration-translation relaxation and dissociation in nonequilibrium gas flows, Phys. Rev. E **83**, 067302 (2011).
[44] A. Aliat, P. Vedula, and E. Josyula, State-specific dissociation modeling with multiquantum vibration-translation transitions, Phys. Rev. E **83**, 037301 (2011).
[45] J. Annaloro and A. Bultel, Vibrational and electronic collisional-radiative model in air for Earth entry problems, Phys. Plasmas **21**, 123512 (2014).
[46] J. G. Kim, O. J. Kwon, and C. Park, Master equation study and nonequilibrium chemical reactions for $H + H_2$ and $H + He$, J. Thermophys. Heat Transfer **23**, 443 (2009).
[47] M. Panesi, R. L. Jaffe, D. W. Schwenke, and T. E. Magin, Rovibrational internal energy transfer and dissociation of $N(^4S_u) + N_2(^1\Sigma_g^+)$ sytem in hypersonic flows, J. Chem. Phys. **138**, 044312 (2013).
[48] M. Panesi, A. Munafò, T. E. Magin, and R. L. Jaffe, Study of the non-equilibrium shock heated nitrogen flows using a rovibrational state-to-state method, Phys. Rev. E **90**, 013009 (2014).
[49] J. G. Kim and I. D. Boyd, Monte Carlo simulation of nitrogen dissociation based on state-resolved cross sections, Phys. Fluids **26**, 012006 (2014).
[50] See Supplemental Material at http://link.aps.org/supplemental/10.1103/PhysRevFluids.1.043401 for additional test cases at different conditions (radiation and flow quantities).

[51] P. A. Gnoffo, R. N. Gupta, and J. L. Shinn, Conservation equations and physical models for hypersonic air flows in thermal and chemical nonequilibrium, NASA Technical Paper 2867 (1989).
[52] L. V. Gurvich, *Thermodynamic Properties of Individual Substances* (CRC Press, Boca Raton, FL, 1994).
[53] K. Fujita, T. Yamada, and N. Ishii, Impact of ablation gas kinetics on hyperbolic entry radiative heating, AIAA paper 2006-1185, 44th AIAA Aerospace Sciences Meeting and Exhibit, Reno, NV, 9–12 January, 2006.
[54] A. Bourdon and P. Vervisch, Study of a low-pressure nitrogen plasma boundary layer over a metallic plate, Phys. Plasmas **4**, 4144 (1997).
[55] L. B. Ibragimova, Recommended rate constants of $CO + O_2$ - reversible - $CO_2 + O$ reactions, Khim. Fiz. **10**, 307 (1991) (in Russian).
[56] T. Gokcen, N_2-CH_4-Ar chemical kinetic model for simulations of atmospheric entry to Titan, AIAA paper 2004-2469, 37th AIAA Thermophysics Conference, Portland, OR, 28 June–1 July, 2004.
[57] D. Bose and G. V. Candler, Thermal rate constants of the $O_2 + N \rightarrow NO + O$ reaction using ab initio $^2A'$ and $^4A''$ potential energy surfaces, J. Chem. Phys. **107**, 6136 (1997).
[58] C. Park, R. L. Jaffe, and H. Partridge, Chemical-kinetic parameters of hyperbolic Earth entry, J. Thermophys. Heat Transfer **15**, 76 (2001).
[59] P. Teulet, J. J. Gonzalez, A. Mercado-Cabrera, Y. Cressault, and A. Gleizes, One-dimensional hydro-kinetic modeling of the decaying arc in air-PA66-copper mixtures: I. Chemical kinetics, thermodynamics, transport and radiative properties, J. Phys. D **42**, 175201 (2009).
[60] C. Park, Rate parameters for electronic excitation of diatomic molecules 1. Electron-impact processes, AIAA paper 2008-1206, 46th AIAA Aerospace Sciences Meeting and Exhibit, Reno, NV, 7–10 January, 2008.
[61] P. V. Marrone and C. E. Treanor, Chemical relaxation with preferential dissociation from excited vibrational levels, Phys. Fluids **6**, 1215 (1963).
[62] J. P. Appleton, M. Steinberg, and D. J. Liquornik, Shock-tube study of carbon monoxide dissociation using vacuum-ultraviolet absorption, J. Chem. Phys. **52**, 2205 (1970).
[63] R. L. Macdonald, A. Munafò, C. O. Johnston, and M. Panesi, State-to-state modeling of CO for Mars entry applications, AIAA 2015-0476, 53rd AIAA Aerospace Sciences Meeting, Kissimmee, FL, 5–9 January, 2015.
[64] R. C. Millikan and D. R. White, Systematics of vibrational relaxation, J. Chem. Phys. **39**, 3209 (1963).
[65] G. V. Candler and R. W. MacCormack, Computation of weakly ionized hypersonic flows in thermochemical nonequilibrium, J. Thermophys. Heat Transfer **5**, 266 (1991).
[66] J. H. Ferziger and H. G. Kaper, *Mathematical Theory of Transport Processes in Gases* (North-Holland, Amsterdam, 1972).
[67] T. E. B. Magin and G. Degrez, Transport properties of partially ionized and unmagnetized plasmas, Phys. Rev. E **70**, 046412 (2004).
[68] E. E. Whiting, An empirical approximation to the Voigt profile, J. Quant. Spectrosc. Radiat. Transfer **8**, 1379 (1968).
[69] C. W. Gear, *Numerical Initial-Value Problems in Ordinary Differential Equations* (Prentice-Hall, Englewood Cliffs, NJ, 1971).
[70] K. Radhakrishnan and A. C. Hindmarsh, Description and use of LSODE, the Livermore solver for ordinary differential equations, NASA Report 1327 (1993).
[71] Y. B. Zel'dovich and Y. P. Raizer, *Physics of Shock Waves and High-Temperature Hydrodynamic Phenomena*, Dover Books on Physics (Dover Publications, Mineola, NY, 2002).
[72] In this case the x axis in Eq. (30) is aligned along the tube radius.